

RESEARCH

Open Access



Prediction of glioma-subtypes: comparison of performance on a DL classifier using bounding box areas versus annotated tumors

Muhaddisa Barat Ali^{1*}, Irene Yu-Hua Gu¹, Alice Lidemar², Mitchel S. Berger³, Georg Widhalm⁴ and Asgeir Store Jakola^{2,5}

Abstract

Background: For brain tumors, identifying the molecular subtypes from magnetic resonance imaging (MRI) is desirable, but remains a challenging task. Recent machine learning and deep learning (DL) approaches may help the classification/prediction of tumor subtypes through MRIs. However, most of these methods require annotated data with ground truth (GT) tumor areas manually drawn by medical experts. The manual annotation is a time consuming process with high demand on medical personnel. As an alternative automatic segmentation is often used. However, it does not guarantee the quality and could lead to improper or failed segmented boundaries due to differences in MRI acquisition parameters across imaging centers, as segmentation is an ill-defined problem. Analogous to visual object tracking and classification, this paper shifts the paradigm by training a classifier using tumor bounding box areas in MR images. The aim of our study is to see whether it is possible to replace GT tumor areas by tumor bounding box areas (e.g. ellipse shaped boxes) for classification without a significant drop in performance.

Method: In patients with diffuse gliomas, training a deep learning classifier for subtype prediction by employing tumor regions of interest (ROIs) using ellipse bounding box versus manual annotated data. Experiments were conducted on two datasets (US and TCGA) consisting of multi-modality MRI scans where the US dataset contained patients with diffuse low-grade gliomas (dLGG) exclusively.

Results: Prediction rates were obtained on 2 test datasets: 69.86% for 1p/19q codeletion status on US dataset and 79.50% for IDH mutation/wild-type on TCGA dataset. Comparisons with that of using annotated GT tumor data for training showed an average of 3.0% degradation (2.92% for 1p/19q codeletion status and 3.23% for IDH genotype).

Conclusion: Using tumor ROIs, i.e., ellipse bounding box tumor areas to replace annotated GT tumor areas for training a deep learning scheme, cause only a modest decline in performance in terms of subtype prediction. With more data that can be made available, this may be a reasonable trade-off where decline in performance may be counteracted with more data.

Keywords: 1p/19q codeletion, IDH genotype, Brain tumor, Ellipse bounding box, Deep learning

Introduction

The most common type of brain tumor is called diffuse glioma and is the reason of 80% of malignant brain tumors [1]. Depending on the aggressiveness of the tumor, World Health Organization (WHO) has categorized them into grades 2-4 where higher grade means more malignant

*Correspondence: barat@chalmers.se

¹ Department of Electrical Engineering, Chalmers University of Technology, Gothenburg, Sweden

Full list of author information is available at the end of the article



© The Author(s) 2022. **Open Access** This article is licensed under a Creative Commons Attribution 4.0 International License, which permits use, sharing, adaptation, distribution and reproduction in any medium or format, as long as you give appropriate credit to the original author(s) and the source, provide a link to the Creative Commons licence, and indicate if changes were made. The images or other third party material in this article are included in the article's Creative Commons licence, unless indicated otherwise in a credit line to the material. If material is not included in the article's Creative Commons licence and your intended use is not permitted by statutory regulation or exceeds the permitted use, you will need to obtain permission directly from the copyright holder. To view a copy of this licence, visit <http://creativecommons.org/licenses/by/4.0/>. The Creative Commons Public Domain Dedication waiver (<http://creativecommons.org/publicdomain/zero/1.0/>) applies to the data made available in this article, unless otherwise stated in a credit line to the data.

tumors, and classified as either astrocytomas and oligodendrogliomas [2]. Traditionally, the grade 2 gliomas are referred to as low-grade gliomas (LGG) and grade 3-4 as high-grade gliomas (HGG). Additionally, recent findings on molecular biomarkers have revised WHO grading to its further subtypes. According to this, isocitrate dehydrogenase (IDH) mutation and 1p/19q codeletion are the hallmarks of the dLGG subtypes which beyond classification also provides important information concerning prognosis and response to therapy [3]. IDH mutations are detected in 70-80% of dLGG [4]. The survival rate for dLGG IDH mutated patients are higher than IDH wild-type patients and plays an important role in prognosis and clinical decisions. This observation has also caused dLGG IDH wild-type with molecular features of glioblastoma to be classified as glioblastomas [5]. Also, in IDH mutated astrocytomas the prognostic importance of extensive cytoreductive surgery is highly convincing [6–9]. Codeletion of 1p/19q is a characteristic of oligodendrogliomas and is a favourable prognostic molecular marker. Since oligodendrogliomas are more sensitive to oncological treatment [8, 9], the role of extensive resection have been discussed and surgical management could be directly affected by knowing dLGG subtype. Therefore, precisely knowing the molecular marker prior to surgery would be of practical value. Recently non-invasive classification methods have shown promising results in prediction of glioma-subtypes based upon pre-operative imaging [10–13]. Non-invasive methods are opening up to discuss tailored therapies that would assist the surgeons and patients in the shared decision making process [14]. However, many challenges remain before bringing these tools into clinical practice.

Accurate tumor boundaries are important, since pixels within tumor boundaries are labeled as tumor for the supervised training of glioma. Using incorrectly labeled pixels for supervised training could lead to reduced test performance of classifier for distinguishing tumors. This pre-processing step helps more accurate supervised training of tumor tissues. Drawing tumor boundaries manually by medical experts is a tedious task often requiring clinicians with anatomical and physiological expertise. Apart from being time consuming task, it makes this procedure prone to intra and inter observer variability [15, 16]. Automatic segmentation is an alternate way to manual annotation. Studies have been conducted for automatic and semi-automatic segmentation of tumors to overcome the time and radiologist constraints e.g. support vector machine [17], decision tree [18], conditional random forest [19], mean shift [20], graph cut algorithm [21], level set method [22] and many more. Recently, DL has gained much attention for its high performance in segmentation of medical images

[23, 24]. The most frequently used model for characterizing visual objects and learning dense characteristics of images is Convolutional Neural Network (CNN) [25]. Relevant works that include segmentation are, among others, U-net [26], patch-based CNN [27] or patch-based multi-scale CNN [28]. However, these methods do not guarantee the quality and could lead to improper or failed segmented boundaries making the segmentation process an ill-defined problem. These approaches are often dependent on the quality and representation of the features and sometimes require physician intervention to identify the most important features, if automatic segmentation fails [25]. Moreover, the devices and protocols used for acquisition of MRIs can vary dramatically on brain scans causing intensity biases and other variations of brain scans in a dataset. These issues may lead to ambiguous ROIs (regions of interest) in segmentation that subsequently affect the diagnosis or classification. Most deep learning segmentation methods are based on supervised learning which requires annotated GT (ground truth) tumor regions for training. Many medical imaging datasets lack the GT tumor annotations that limits the use of those datasets. It is worth noting that using bounding boxes for object tracking [29] and classification have been successfully applied on visual images to bypass the ambiguity issues in automatic segmentation. However, this idea is rarely applied in MRI-based diagnosis.

For glioma classification, DL offers an automatic way to learn features. In the past few years, several DL methods have been successfully introduced for such applications. Chang et al. [30] introduced a method that uses residual CNNs for the prediction of IDH mutation using four modalities of MRI data. Li et al. [31] trained a 6 layer CNN for tumor segmentation on GT tumor data. Then features from the last fully connected layer were size normalized by Fisher vector coding followed by a SVM classifier for IDH mutation prediction. Liang et al. [32] suggested to use more advanced DenseNets using 3D MRI scans for IDH mutation prediction and obtained good performance for glioma grading. Yogananda et al. [13] proposed an approach on training from scratch 3D-Dense-UNets for performing classification and segmentation simultaneously for IDH mutation status and proved that network trained on FLAIR-MRIs gives the same performance as when trained on multi-contrast MRIs (T2, FLAIR and T1ce) on TCGA dataset with 214 patients. Then, in [12] they used the same trained network in transfer learning for 1p/19q codeletion prediction with 368 patients with T2-MRIs.

Our work is mainly motivated for the prediction of diffuse glioma-subtypes by shifting the paradigm in supervised training by using tumor ROIs specified by bounding box areas e.g., ellipse shaped around the

tumors instead of accurate tumor boundaries. Although, manual GT annotation has been the best way to allocate ROIs, it is a time consuming process and needs medical expertise. Likewise, automatic segmentation comes with its own challenges because it is an ill-defined problem and doesn't always guarantee accurate tumor boundaries. Inspired by computer vision community's successful research on visual object tracking and classification using bounding boxes, this paper attempts to shift the study through an alternate paradigm for MRI-tumor subtypes prediction where supervised training in DL scheme utilizes the bounding box areas on MRI medical data. To the best of our knowledge, it is the first time that such a strategy has been successfully adopted for diffuse glioma-subtype prediction and comparing the performance to those trained on GT tumor areas. In this work, we used tight ellipse bounding boxes for locating brain tumor areas, in such a way that surrounding tissue does not cause much deterioration of the features in identifying the subtypes of diffuse gliomas. We show that a glioma-subtype classifier trained by using tumor bounding box areas may achieve comparable performance, with a slight performance degradation of about 3.0% averaged on 2 dataset results.

Overview of a DL classification scheme: 2D multi-stream CNN classifier

We adopted the classifier from a previous work [46] as a DL prediction scheme for the feature learning and classification of glioma-subtypes. Considering the moderate and small sizes of training datasets, we choose a 2D MRI slice-based classifier as: (a) due to the curse of dimensionality, one has to significantly increase the size of MRI training dataset to avoid the over-fitting, if high

dimensional 3D volume data is used as the input; (b) using slice based approach could significantly reduce the computations by only processing a few slices containing the tumor. For the sake of convenience to the readers, a brief overview of the classifier is given in Fig. 1. The deep network uses number of streams based on the MRI modalities used. Each stream consists of 6 convolutional layers with filter size 3 × 3 in each layer. Let the feature maps with their modality specific characteristics from all streams be denoted as F_1, F_2, F_3 and F_4 respectively. These features are extracted from the last convolutional layers followed by the feature information fusion layers, where the features are fused together as $F = F_1 \odot F_2 \odot F_3 \odot F_4$ at aggregation layer and are compactly represented at bilinear layer as $y = F^T F$. The final refined feature map is followed by 2 fully connected layers with random initialization and dropout regularization that ends at a final layer for glioma-subtype class prediction.

Proposed method

In this section, we describe the proposed approach where tumor ROIs are employed as the inputs for training the DL scheme. First, the approach for tumor subtype prediction and performance comparison are described. Then the selection of ellipse bounding boxes as tumor ROIs is described.

Glioma-subtype prediction based on the DL scheme trained by tumor ROIs

The proposed strategy introduces ellipse shaped bounding boxes as ROIs to occupy all the tumor areas. Figure 2 shows the block diagram of the pipeline for glioma-subtype prediction based on two datasets: TCGA (public

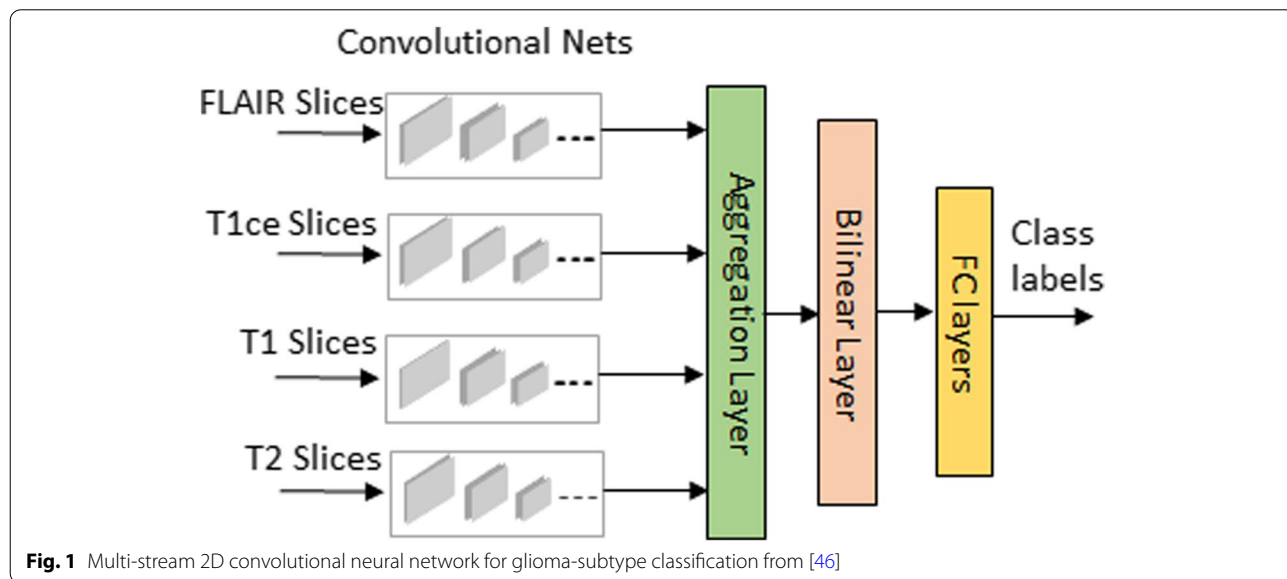
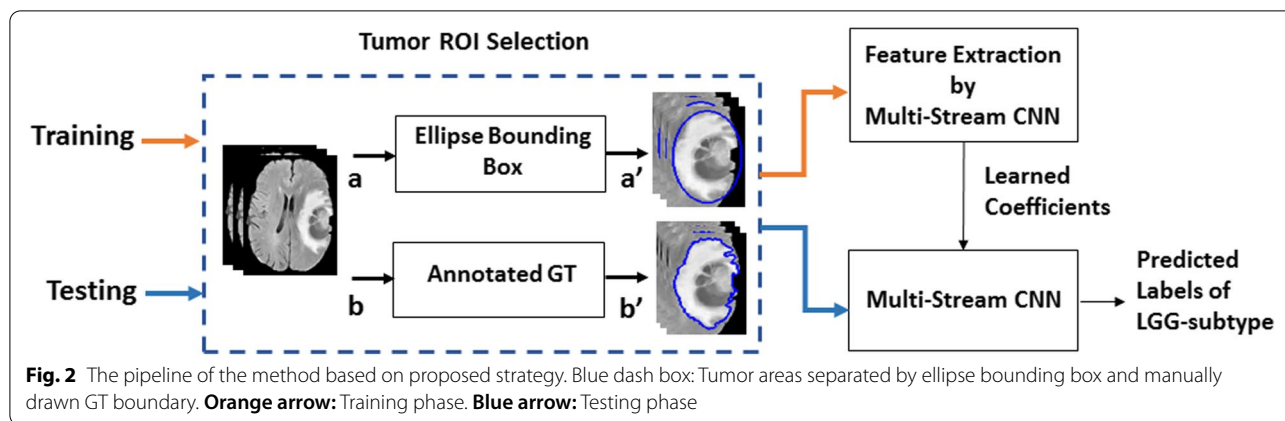


Fig. 1 Multi-stream 2D convolutional neural network for glioma-subtype classification from [46]



dataset) and US (clinical dataset). Two modalities (FLAIR and T1ce) from US dataset are used for case study-A and four modalities (T1, T2, FLAIR and T1 contrast enhanced (T1ce)) are used from TCGA dataset for case study-B. In order to find how well the proposed strategy performs compared to that of using GT annotated data, a comparison of the performance of the classifier was examined against each training data type. Firstly, the classifier was trained and tested on ellipse tumor bounding box data. Secondly, the same experiment was repeated by training on the manually annotated GT tumor data.

From Fig. 2, input 2D multi-modality MRIs are fed to tumor ROI selection block, as shown in blue dotted box. When this block receives input 2D MR images from point **a**, it processes them to output point **a'** by introducing a tight ellipse bounding box around the tumor area. Then, the multi-stream 2D Convolutional neural network is trained on the selected ROIs to learn features from each of the corresponding multi-modality MRIs. After the model is trained, during testing phase, the prediction is obtained from the test data with ellipse tumor bounding box areas obtained at point **a'**. To check the classification performance with that trained by GT annotated data, MRIs are given at point **b** for GT ROIs selection and are processed further at point **b'** in the blue dashed block. Following this, the network is trained and tested accordingly. Finally, the test accuracy on both the data types are compared. This procedure is repeated separately for each of the datasets.

Tumor ROI selection: ellipse bounding box

In this part, we shall give further details of the blue dashed box from Fig. 2. DL is computationally expensive and brain MRIs are complex that consist of many anatomical details. Typically, a full 2D slice image isn't useful to detect subtype of gliomas on molecular level. The tumor areas can be better focused for a faster and more

accurate model training. As brain tumors show great variations in shape, size and intensity, a tight elliptical shaped bounding box is introduced surrounding the tumor. In this work, tight elliptical bounding boxes are obtained manually. As mentioned in [34–36], we believe that this strategy helps to capture certain amount of information not only in tumor region but also information from the surrounding tissue that may not cause a major problem in recognition of glioma-subtypes. Tumor area selection using ellipse bounding box is shown in Fig. 3 for 3 directional views of a FLAIR-MRI. As FLAIR-MRIs present visually better tumor contrast with its surrounding tissues, a tight ellipse bounding box is drawn manually with the help of 8 points whose positions are adjusted in accordance with the shape of the tumor. The binary tumor mask generated from this procedure is then applied to the other modalities of the patient to generate ellipse shaped tumor data for all modalities.

From Fig. 2, the other way to separate the tumor region is by simply masking out the tumor area if the GT annotation is available for the dataset. This generates GT data with manually drawn tumor boundary discarding the surrounding non-tumor tissues. In Fig. 4, examples on ellipse boxed tumor area and GT annotated area are shown for FLAIR-MRI modality.

Results and comparisons

Setup: Experiments were implemented using Keras library [33] with Tensor Flow backend on a workstation with Intel-i7 3.40GHz CPU, 48G RAM and an NVIDIA Titan Xp 12GB GPU. By tuning the network carefully through experiments, different parameters were selected. Learning rate was set to $1.0e^{-4}$. Optimizer used was *Adagrad*. Batch size was set to 16. We used *L2*-norm regularization with the value of parameter selected as $1.0e^{-4}$ for convolutional layers of each stream. The categorical cross-entropy was used as a loss function for

evaluating the final performance. Here, we adapted early stopping strategy when the best validation performance was achieved. The random dropout rate was set to 0.5 for two fully connected layers for TCGA dataset and 0.6 for US dataset. Simple data augmentations such as horizontal flipping and random rotation (maximum at 10°) were used by Keras function *ImageDataGenerator* in real time to minimize the memory usage during training.

Datasets: Two datasets were used in the experiments for glioma-subtype prediction as shown in Table 1. One is a clinical dataset from Department of Neurosurgery,

University of San Francisco, California (UCSF), referred to the US dataset in this paper. The other is TCGA dataset from TCGA-GBM (n = 101) [37] and TCGA-LGG (n = 66) [38] with IDH genotype labels. The MRI-modalities and the number of patients used for each of the datasets are given in Table 1(a). Unlike TCGA dataset, US dataset consists of only dLGG (Who grade 2) with the typical appearance of non-enhancing hyper-intensive ROIs in FLAIR images and without significant contrast enhancement. The ground truth annotation or tumor mask for TCGA dataset is publicly available. For US dataset, tumor

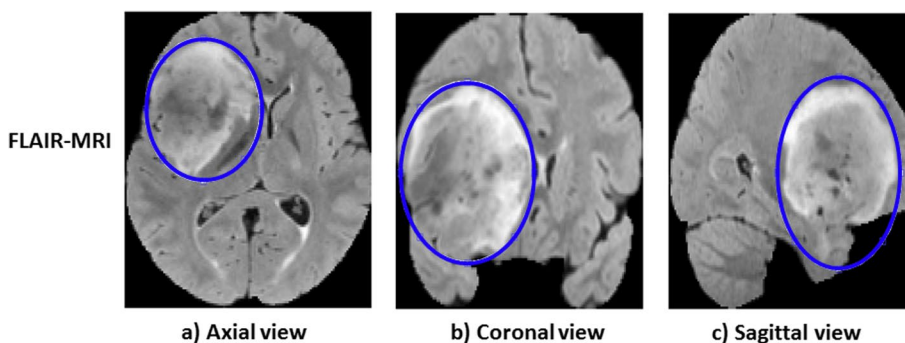


Fig. 3 Illustration of selection of ROIs with tight ellipse bounding box for a FLAIR-MRI from US dataset for all three directional views. The blue line defines the tumor area contour

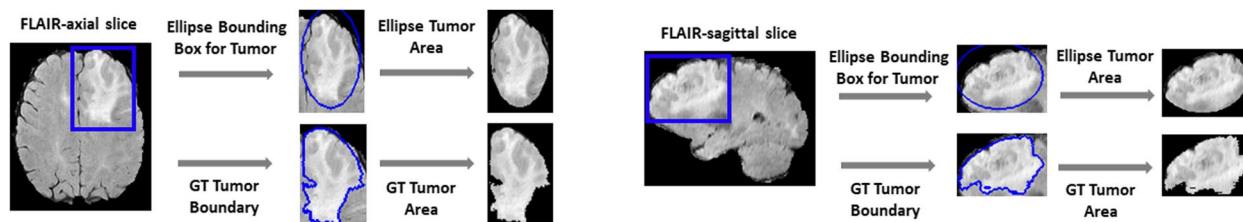


Fig. 4 An example of TCGA dataset from IDH mutation class. Separation of ROIs is shown in both ways (using ellipse bounding box and GT) on FLAIR modality. **Left:** Axial view. **Right:** Sagittal view

Table 1 Summary of Two Datasets (a) Number of 3D scans in each datasets. (b) Description of data for two case studies

(a)				
Dataset	T1ce	FLAIR	T1	T2
US	75	75	-	-
TCGA	167	167	167	167
(b)				
Case Study	Glioma Subtype	#3D/2D*(Training)	#3D/2D*(Validation)	#3D/2D*(Testing)
A	1p/19q cod	25/450	8/144	9/162
	1p/19q non-cod	20/360	6/108	7/126
B	IDH-mut	33/594	11/198	11/198
	IDH-wt	68/612	22/198	22/198

*Excluded with augmented slice images

boundaries were drawn manually through the help of 3D slicer tool (v4.10.2) [39] and all annotation was controlled by the senior medical doctor (ASJ), having extensive experience in LGG research and segmentation. The datasets consist of 3D brain scans where 2D image slices from all three views (axial, sagittal and coronal) were extracted for our experiments. Each dataset was split patient wise into 3 sets: training (60%), validation (20%) and testing (20%) such that no images of a patient from one set is used in another. For each run, patients were selected randomly for each of the sets and the results of multiple runs were averaged for the final performance evaluation.

The details of two case studies are shown in Table 1(b). For case study-A, we used US dataset that has two modalities T1ce-MRI and FLAIR-MRI for prediction of LGG with 1p/19q codeletion and non-codeletion. Here, 42 patients are 1p/19q codeleted and 33 patients are non-codeleted. Observing that the tumor size varies from small to medium in different subjects, 6 slices for each of the views (axial, coronal, sagittal) have been extracted from a 3D scan. Keeping the slice with the biggest tumor area as centre slice, other slices were extracted from both sides. For case study-B, we used TCGA dataset with four modalities (T1ce, FLAIR, T1 and T2) for classifying IDH genotype. For this case study, one can see that 55 patients are labeled as IDH-mutated and 112 patients as IDH-wild type from Table 1(b). Unlike Case study-A, this dataset has large class imbalance for IDH genotype. Therefore, 3 times more slices have been extracted for patients with IDH mutation i.e; 3 for each view for IDH wild-type and 6 for each view for IDH-mutation.

Criteria: To evaluate the performance of diffuse glioma-subtype prediction on both case studies, we used accuracy, precision, specificity, sensitivity/recall and F1-score as the evaluation criteria on the test results averaged over 5 runs. The metrics computed were based on the following four kinds of samples:

True positive (TP): 1p/19q codeleted/IDH mutated glioma was correctly classified as 1p/19q codeleted/ IDH mutated.

False positive (FP): 1p/19q non-codeleted/IDH wild-type glioma was incorrectly classified as 1p/19q codeleted/ IDH mutated.

True negative (TN): 1p/19q non-codeleted/IDH wild-type glioma was correctly classified as 1p/19q non-codeleted/ IDH wild-type.

False negative (FN): 1p/19q codeleted/ IDH mutated glioma was incorrectly classified as 1p/19q non-codeleted/ IDH wild-type.

defined as accuracy, specificity and sensitivity.

$$\text{Accuracy} = \frac{TP + TN}{TP + FP + TN + FN}, \quad \text{Precision} = \frac{TP}{TP + FP}$$

$$\text{Specificity} = \frac{TN}{FP + TN}, \quad \text{Sensitivity/Recall} = \frac{TP}{TP + FN}$$

$$\text{F1-score} = 2 \times \frac{(\text{Recall} \times \text{Precision})}{\text{Recall} + \text{Precision}}$$

Pre-processing: This step has an impact on the performance. The clinical 3D volume data in US dataset was unregistered. So, the anatomical images from FLAIR and T1ce scans were registered to 1mm MNI space template. In addition to this, the bias field correction and skull-stripping steps were performed using FSL [40] and ANTs [41] tools. The TCGA data needs no pre-processing and is readily available as skull-stripped and co-registered with IDH genotype labels. To save computation, slices were rescaled to a 128×128 size and then normalized to range [0,1].

Results on test sets

First we evaluated the procedure on both case studies/datasets using the classification scheme with the ellipse bounding box tumor data.

Case-A: In this case, US dataset containing only dLGG, was studied. As the data size is small, to help the network learn the features, we used a higher rate of dropout (60%) in the fully connected layers as a regularization effect. Hence, the training and validation curves show up some variations. Figure 5 shows the training and validation curves as a function of epochs for 5th run from Table 2(a). Early stopping was applied as one can see from the curve that the validation accuracy did not improve after epoch = 67, hence the coefficients of DL scheme were frozen from this epoch. The testing accuracy obtained was 72.57% at this epoch. Table 2(a) shows the results on the test dataset. The average test accuracy for 1p/19q prediction is 69.86%. The average sensitivity 74.20% is higher than the specificity 64.60%, because patients with 1p/19q codeletion are more frequent in this dataset. This resulted an average F1-score of 73.51%.

Case-B: As observed in Fig. 5 for 4th run from Table 2(b), the test accuracy obtained was 82.58% at epoch = 76. Observing the average prediction result of this case study from Table 2(b), the average sensitivity (72.32%) lower than the average specificity (86.65%) because of the high class imbalance in this dataset between IDH mutated and IDH wild-type class. The average accuracy is 79.50% and average F1-score as 78.06%. Here, due to large class imbalance F1-score can be considered a better metric for the evaluation.

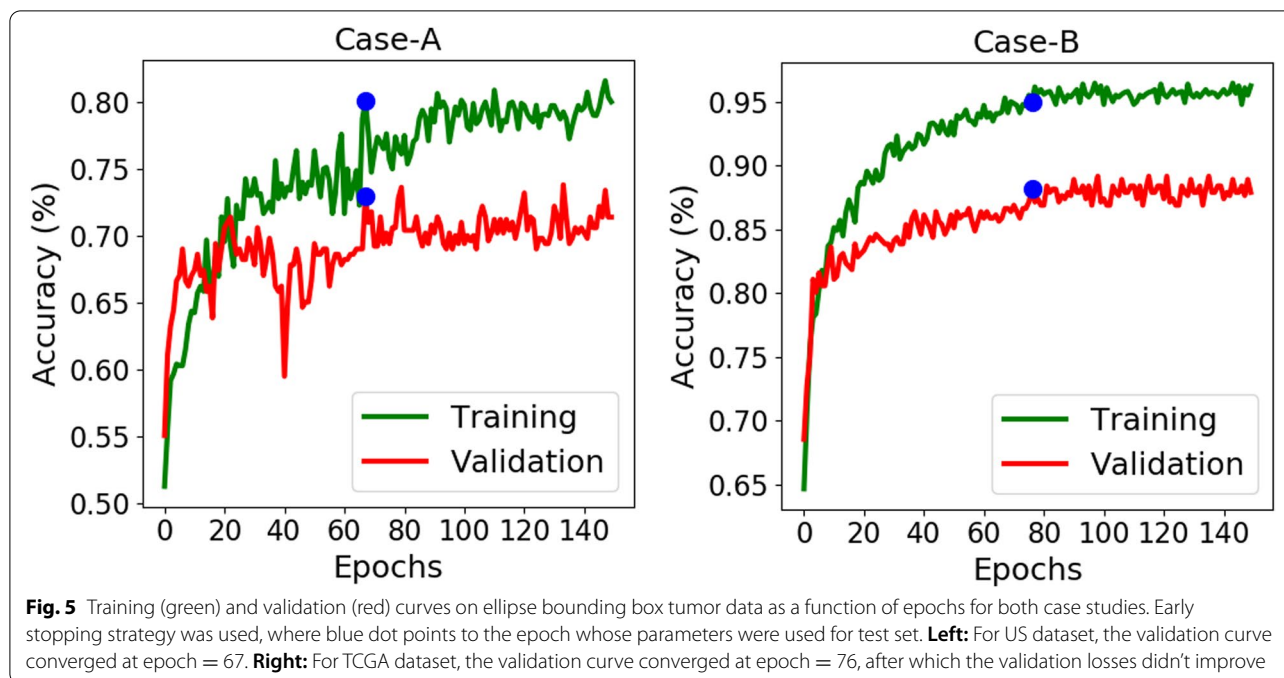


Table 2 Comparison of the average test results for diffuse glioma-subtypes using ellipse bounding box tumor data for 5 runs. The highest values obtained in each run are displayed in bold text. (a) Case-A for US dataset (1p/19q prediction). (b) Case-B for TCGA dataset (IDH genotype)

Run	Dataset	Accuracy (%)	Precision (%)	Sensitivity(%)	Specificity(%)	F1-Score(%)
(a) Case-A: Prediction Result on Ellipse Bounding Tumor Areas						
1		65.97	70.00	69.14	61.90	69.57
2	US	71.53	74.10	75.93	65.87	75.00
3	(1p/19q Codel/	68.06	72.73	69.14	66.67	70.90
4	Non-Codel)	71.18	74.25	76.54	65.87	75.38
5		72.57	73.45	80.25	62.70	76.70
	Average(σ)	69.86 (2.46)	72.91(1.55)	74.20(4.39)	64.60 (1.92)	73.51(2.76)
(b) Case-B: Prediction Result on Ellipse Bounding Tumor Areas						
1		79.55	85.03	71.71	87.37	77.80
2	TCGA	76.01	78.45	71.72	80.30	74.93
3	(IDH mut/	80.30	86.23	72.73	87.88	78.91
4	wild-type)	82.58	88.69	75.25	89.90	81.42
5		79.04	85.80	70.20	87.88	77.22
	Average(σ)	79.50(2.12)	84.84(3.42)	72.32(1.67)	86.65(3.28)	78.06 (2.13)

Comparison of prediction results with the annotated GT data

We then compare the prediction performance through otherwise identical DL pipeline, but using annotated GT test sets where the DL scheme was trained by annotated GT training data. The summary of the average performance metrics (all averaged over 5 runs through same sequence of data re-partition for each run and re-training the DL scheme) is shown in Fig. 6. Observing the results

for the difference in performance in Table 3, one can see that the average test accuracy with ellipse bounding box has resulted in slightly degraded performance on the test datasets, by 2.92% in US dataset (with difference of 1.85% in sensitivity and 3.97% in specificity) and by 3.23% in TCGA dataset (with difference of 3.05% in sensitivity and 3.13% in specificity).

To further examine the difference between the ellipse bounding box areas and the GT tumor boundaries

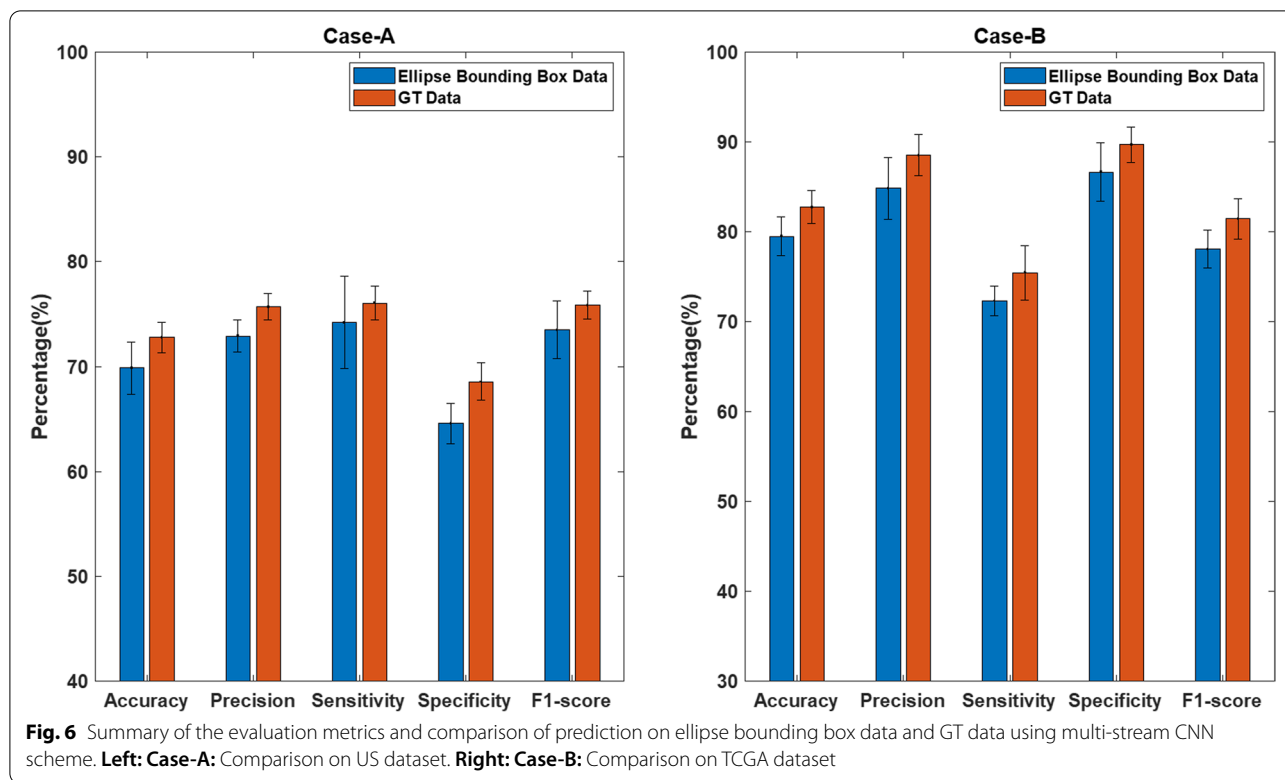


Table 3 Performance difference on average prediction results (over 5 runs) by using GT tumor data and ellipse tumor bounding box data for training, where the standard deviation is included in (·) after each performance value

Case Study	Tumor Area	Av. Acc.(σ)	Av. Sen.(σ)	Av. Spec.(σ)
A	Ellipse	69.86(2.46)	74.20(4.39)	64.60(1.92)
	GT	72.78(1.45)	76.05(1.63)	68.57(1.78)
Difference		2.92(1.45)	1.85(1.78)	3.97(1.63)
B	Ellipse	79.50(2.12)	86.65(3.28)	72.32(1.67)
	GT	82.73(1.82)	89.70(2.00)	75.45(3.04)
Difference		3.23(0.3)	3.05(1.28)	3.13(1.37)

marked by medical experts (see Fig. 7), the average tumor dice scores were computed on the training sets of the two datasets. The dice score is defined as $D = \frac{2|X \cap Y|}{|X| + |Y|}$, where X is the tumor image with pixels within the ellipse area, and Y is the GT tumor image with pixels within the GT tumor boundaries. Table 4 shows the average of dice scores on the training sets which indicates that some non-tumor pixels were included in ellipse bounding boxes. This is expected as tumor shape is non-elliptical (see Fig. 7, where both GT tumor areas and the ellipse bounding boxes are marked on images). This is rather encouraging, as it indicates that replacing medical

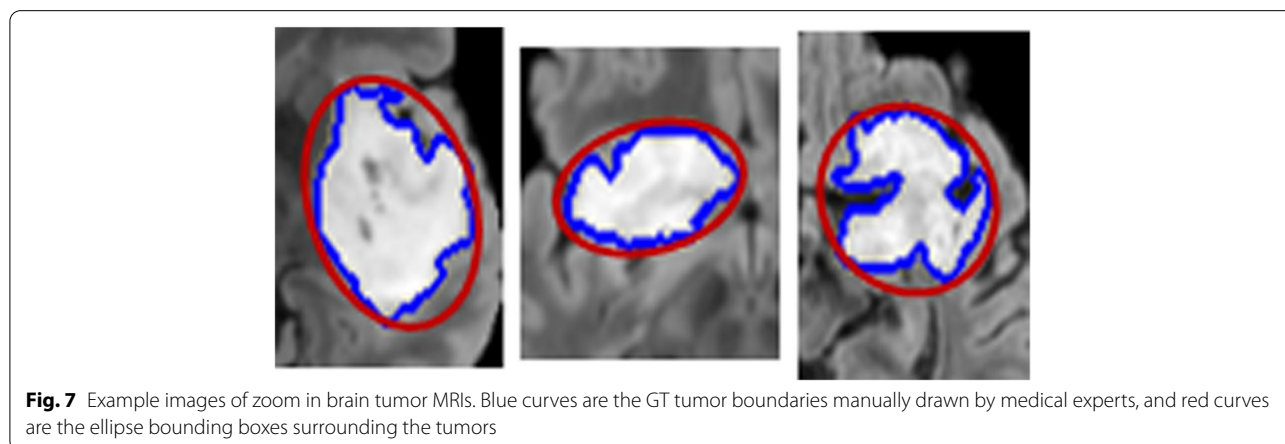


Table 4 Averaging tumor dice score calculated between medical experts' marked GT tumor areas and ellipse tumor bounding box areas

Case Study	Dataset	Av. Dice score (σ)
A	US	0.8046 (0.0652)
B	TCGA	0.8279 (0.0514)

experts' marked GT tumor areas by ellipse bounding box areas in the training has resulted in small performance reduction in the classification (see Table 3) on test sets. Further, it is worth mentioning that medical experts' marked GT tumors would be the best results that any automatic segmentation could generate, and hence, Table 3 equivalently is to have compared ours with the network trained by using the best possible segmented tumor areas.

Discussion

Some insights can be obtained from our experimental results using the proposed strategy:

- Using ellipse bounding box strategy showed good performance on two different datasets for diffuse glioma-subtype prediction: US dataset for WHO grade 2 dLGGs (to predict 1p/19q codeletion/non-codeletion) and TCGA data (to predict IDH mutation/wild-type). It is worth mentioning that other shape of bounding boxes, e.g., rectangles [42], can also be selected. We chose elliptical shape to reduce the false positive tumor pixels around the corner areas of rectangles, so that fewer non-tumor pixels would be wrongly labeled and subsequently used for supervised training of tumors.
- The average test accuracy of US dataset is lower comparatively because it consists of only dLGG without significant contrast enhancement. The other reason is rather smaller dataset size. On the other hand, TCGA dataset performs better probably because it consists of patients with both LGG and HGG groups and since the task of IDH detection is easier than that of 1p/19q codeletion.
- Average test accuracy on both the datasets, showed slight degradation in performance of about 3% on the ROIs selected by the proposed strategy. This degradation appears as a trade-off between time and personnel demanding task of manual annotation and a slightly reduced performance and can perhaps be counteracted by having more training data available using this approach.
- Several studies have reported their classification performance on 1p/19q codeletion status using data

from both diffuse LGGs and HGGs [10, 12]. Tumors of higher grades typically looks very different and the data is interrelated to molecular markers that it might cause a significant boost in performance. In our study, US dataset consisted of only dLGGs (WHO grade 2) that appears with non-enhanced hyperintensive tumor areas making it more challenging to categorize.

- For IDH genotype, there are some recent studies with superior performance based upon segmentation with more patients and having better balance between classes [13, 43]. Although the scope of the paper was not to compare with them or to create a state-of-the-art prediction. Still, our aim was to study whether a simpler set-up would produce comparable results using a relevant method [44, 45]. Based upon our findings, we believe it is reasonable to use the strategy of tight bounding box and to increase the amount of data available in addition to make it simple and clinical relevant. A significant increase in training data may also actually improve performance in future experiments.

Limitations: One effective way of further improving the performance is to increase the size of training dataset since accurate feature characterization in DL is dependent on using large number of training data. In our study, the overall size and the imbalance in the datasets for two classes caused one class with relatively lower performance that has affected the average test performances. One solution is to add synthetic MRI slices in the training dataset through, e.g., employing Generative Adversarial Networks. Furthermore, automatic algorithms instead of manual selection of ellipse bounding box can improve the practical application and could be further studied.

Conclusion

Manual annotation of MRI tumor areas is time consuming and requires considerable medical expertise. Also, automatic segmentation is ill-defined due to MR image differences from multiple imaging centers. More data is desirable in radiogenomic analysis but many available datasets lack expert tumor boundary annotation. An alternate paradigm of using tumor ROIs by tight ellipse bounding boxes is studied. Our study has shown that it is feasible to use ellipse shape tumor bounding box areas in place of annotated tumor GT areas for supervised trained DL, leading to good performance (average test accuracy of 69.86% for predicting 1p/19q codeletion and 79.50% for IDH mutation) with a small performance degradation (approximately 3.0%). Our results show a possible way to trade-off between training DL schemes using manually annotated tumors

and using bounding boxes surrounding the tumors, in terms of saving annotation time and accepting a small performance degradation (about 3%). Our results demonstrate that the tissues surrounding the tumor regions in the ellipse bounding box areas do not cause a major deterioration of performance in predicting the glioma-subtypes.

Abbreviations

MRI: Magnetic Resonance Image; dLGG: Diffuse low grade glioma; GT: Ground Truth; DL: Deep Learning; ROIs: Regions of Interest; IDH: Isocitrate dehydrogenase; WHO: World Health Organization; GBM: Glioblastoma; CNN: Convolutional Neural Network; FLAIR: Fluid-Attenuated Inversion Recovery; T1ce: T1 weighted MRI with contrast enhanced.

Acknowledgements

The results in this paper are in part based upon the MRI data from Department of Neurosurgery, UCSF, USA and by the TCGA Research Network: <https://www.cancer.gov/tcga>.

Authors' contributions

MBA developed the method, performed experiments and did the manuscript writing. IYHG participated in the design of experiments, exchanged ideas and participated in discussion on the method and experimental results, as well as paper drafting. MSB and GW provided US dataset. US data was annotated by AL under the supervision of ASJ. ASJ also provided medical background, contributed in exchange of ideas and paper drafting. All authors have read and approved the final draft.

Funding

Open access funding provided by Chalmers University of Technology. The work of Asgeir Jakola was supported by The Swedish Research Council VR under the grant 2017-00944.

Availability of data and materials

Datasets used in the paper was downloaded from TCGA-GBM Collection <https://doi.org/10.7937/K9/TCIA.2017.KLXWJ1Q> and TCGA-LGG Collection <https://doi.org/10.7937/K9/TCIA.2017.GJQ7R0EF>.

Declarations

Ethics approval and consent to participate

This research has been approved by ethical committee of Western Sweden (Dnr: 702-18) and by institutional review board of University of California, San Francisco (UCSF) for US dataset. Ethics committee approval and informed consent of patients were not required for TCGA dataset, since the MRI data has been obtained from a public dataset. We are strictly in accordance with the data access policies and publication guidelines of the TCGA dataset.

Consent for publication

Not applicable.

Competing interests

The authors declare that they have no competing interests.

Author details

¹Department of Electrical Engineering, Chalmers University of Technology, Gothenburg, Sweden. ²Department of Clinical Neuroscience, University of Gothenburg, Gothenburg, Sweden. ³Department of Neurological Surgery, University of California San Francisco, San Francisco, USA. ⁴Department of Neurosurgery, Medical University of Vienna, Vienna, Austria. ⁵Department of Neurosurgery, Sahlgrenska University Hospital, Gothenburg, Sweden.

Received: 6 October 2021 Accepted: 7 April 2022

Published online: 19 May 2022

References

- Goodenberger ML, Jenkins RB. Genetics of adult glioma. *Cancer Genet.* 2012;205(12):613–21.
- Louis DN, Perry A, Reifenberger G, Von Deimling A, Figarella-Branger D, Cavenee WK, Ohgaki H, Wiestler OD, Kleihues P, Ellison DW. The 2016 world health organization classification of tumors of the central nervous system: a summary. *Acta Neuropathol.* 2016;131(6):803–20.
- Fuller CE, Perry A. Molecular diagnostics in central nervous system tumors. *Adv Anat Pathol.* 2005;12(4):180–94.
- Parsons DW, Jones S, Zhang X, Lin JC-H, Leary RJ, Angenendt P, Mankoo P, Carter H, Siu I-M, Gallia GL, et al. An integrated genomic analysis of human glioblastoma multiforme. *Science.* 2008;321(5897):1807–12.
- Louis DN, Perry A, Wesseling P, Brat DJ, Cree IA, Figarella-Branger D, Hawkins C, Ng H, Pfister SM, Reifenberger G, et al. The 2021 WHO classification of tumors of the central nervous system: a summary. *Neuro-Oncol.* 2021;23(8):1231–51.
- Beiko J, Suki D, Hess KR, Fox BD, Cheung V, Cabral M, Shonka N, Gilbert MR, Sawaya R, Prabhu SS, et al. IDH1 mutant malignant astrocytomas are more amenable to surgical resection and have a survival benefit associated with maximal surgical resection. *Neuro-Oncol.* 2014;16(11):81–91.
- Cordier D, Goz  C, Sch delin S, Rigau V, Mariani L, Duffau H. A better surgical resectability of WHO grade II gliomas is independent of favorable molecular markers. *J Neuro-Oncol.* 2015;121(1):185–93.
- Wijnenga MM, van der Voort SR, French PJ, Klein S, Dubbink HJ, Dinjens WN, Atmodimedjo PN, de Groot M, Kros JM, Schouten JW, et al. Differences in spatial distribution between WHO 2016 low-grade glioma molecular subgroups. *Neuro-Oncol Adv.* 2019;1(1):001.
- Delev D, Heiland DH, Franco P, Reinacher P, Mader I, Staszewski O, Lassmann S, Grau S, Schnell O. Surgical management of lower-grade glioma in the spotlight of the 2016 WHO classification system. *J Neuro-Oncol.* 2019;141(1):223–33.
- Zhou H, Chang K, Bai HX, Xiao B, Su C, Bi WL, Zhang PJ, Senders JT, Vali res M, Kavouridis VK, et al. Machine learning reveals multimodal MRI patterns predictive of isocitrate dehydrogenase and 1p/19q status in diffuse low- and high-grade gliomas. *J Neuro-Oncol.* 2019;142(2):299–307.
- Akkus Z, Ali I, Sedl r J, Agrawal JP, Parney IF, Giannini C, Erickson BJ. Predicting deletion of chromosomal arms 1p/19q in low-grade gliomas from MRI images using machine intelligence. *J Digit Imaging.* 2017;30(4):469–76.
- Yogananda CGB, Shah BR, Yu FF, Pinho MC, Nalawade SS, Murugesan GK, Wagner BC, Mickey B, Patel TR, Fei B, et al. A novel fully automated MRI-based deep-learning method for classification of 1p/19q co-deletion status in brain gliomas. *Neuro-Oncol Adv.* 2020;2(Supplement_4):42–8.
- Bangalore Yogananda CG, Shah BR, Vejdani-Jahromi M, Nalawade SS, Murugesan GK, Yu FF, Pinho MC, Wagner BC, Mickey B, Patel TR, et al. A novel fully automated MRI-based deep-learning method for classification of IDH mutation status in brain gliomas. *Neuro-Oncology.* 2020;22(3):402–11.
- Corell A, Guo A, Vecchio TG, Ozanne A, Jakola AS. Shared decision-making in neurosurgery: a scoping review. *Acta Neurochir.* 2021;163:1–12.
- B  HK, Solheim O, Jakola AS, Kvistad K-A, Reinertsen I, Berntsen EM. Intra-rater variability in low-grade glioma segmentation. *J Neuro-Oncol.* 2017;131(2):393–402.
- White DR, Houston AS, Sampson WF, Wilkins GP. Intra- and interoperator variations in region-of-interest drawing and their effect on the measurement of glomerular filtration rates. *Clin Nucl Med.* 1999;24(3):177–81.
- Bauer S, Nolte L-P, Reyes M. Fully automatic segmentation of brain tumor images using support vector machine classification in combination with hierarchical conditional random field regularization. In: International Conference on Medical Image Computing and Computer-Assisted Intervention. Springer; 2011. p. 354–61.
- Meier R, Bauer S, Slotboom J, Wiest R, Reyes M. A hybrid model for multimodal brain tumor segmentation. *Multimodal Brain Tumor Segmentation.* 2013;31:31–7.
- Tustison NJ, Shrinidhi K, Wintermark M, Durst CR, Kandel BM, Gee JC, Grossman MC, Avants BB. Optimal symmetric multimodal templates and concatenated random forests for supervised brain tumor segmentation (simplified) with ants. *Neuroinformatics.* 2015;13(2):209–25.
- Mahalakshmi DM, Sumathi S. Brain tumour segmentation strategies utilizing mean shift clustering and content based active contour segmentation. *IJIVP.* 2019;9(4):2002–8.

21. Birkbeck N, Cobzas D, Jagersand M, Murtha A, Keszttyues T. An interactive graph cut method for brain tumor segmentation. In: 2009 Workshop on Applications of Computer Vision (WACV). IEEE; 2009. p. 1–7.
22. Thapaliya K, Pyun J-Y, Park C-S, Kwon G-R. Level set method with automatic selective local statistics for brain tumor segmentation in mr images. *Comput Med Imaging Graph.* 2013;37(7-8):522–537.
23. Litjens G, Kooi T, Bejnordi BE, Setio AAA, Ciompi F, Ghafoorian M, Van Der Laak JA, Van Ginneken B, Sánchez CI. A survey on deep learning in medical image analysis. *Med Image Anal.* 2017;42:60–88.
24. Litjens G, Kooi T, Bejnordi BE, Setio AAA, Ciompi F, Ghafoorian M, Van Der Laak JA, Van Ginneken B, Sánchez CI. A survey on deep learning in medical image analysis. *Med Image Anal.* 2017;42:60–88.
25. Olabarrriaga SD, Smeulders AW. Interaction in the segmentation of medical images: A survey. *Med Image Anal.* 2001;5(2):127–42.
26. Dong H, Yang G, Liu F, Mo Y, Guo Y. Automatic brain tumor detection and segmentation using u-net based fully convolutional networks. In: Annual Conference on Medical Image Understanding and Analysis. Springer; 2017. p. 506–517.
27. Pereira S, Pinto A, Alves V, Silva CA. Brain tumor segmentation using convolutional neural networks in mri images. *IEEE Trans Med Imaging.* 2016;35(5):1240–51.
28. Havaei M, Davy A, Warde-Farley D, Biard A, Courville A, Bengio Y, Pal C, Jodoin P-M, Larochelle H. Brain tumor segmentation with deep neural networks. *Med Image Anal.* 2017;35:18–31.
29. Mousavian A, Anguelov D, Flynn J, Kosecka J. 3d bounding box estimation using deep learning and geometry. In: Proceedings of the IEEE Conference on Computer Vision and Pattern Recognition: IEEE; 2017. p. 7074–82.
30. Chang K, Bai HX, Zhou H, Su C, Bi WL, Agbodza E, Kavouridis VK, Senders JT, Boaro A, Beers A, et al. Residual convolutional neural network for the determination of idh status in low-and high-grade gliomas from mr imaging. *Clin Cancer Res.* 2018;24(5):1073–81.
31. Li Z, Wang Y, Yu J, Guo Y, Cao W. Deep learning based radiomics (dlr) and its usage in noninvasive idh1 prediction for low grade glioma. *Sci Rep.* 2017;7(1):1–11.
32. Liang S, Zhang R, Liang D, Song T, Ai T, Xia C, Xia L, Wang Y. Multimodal 3d densenet for idh genotype prediction in gliomas. *Genes.* 2018;9(8):382.
33. Chollet F. Keras. GitHub repository. 2015;5bcac37. <https://github.com/fchollet/keras>.
34. Cheng J, Huang W, Cao S, Yang R, Yang W, Yun Z, Wang Z, Feng Q. Enhanced performance of brain tumor classification via tumor region augmentation and partition. *PLoS ONE.* 2015;10(10):0140381.
35. Matas J, Chum O, Urban M, Pajdla T. Robust wide-baseline stereo from maximally stable extremal regions. *Image Vis Comput.* 2004;22(10):761–7.
36. Mikolajczyk K, Tuytelaars T, Schmid C, Zisserman A, Matas J, Schaffalitzky F, Kadir T, Van Gool L. A comparison of affine region detectors. *Int J Comput Vis.* 2005;65(1):43–72.
37. Bakas S, Akbari H, Sotiras A, Bilello M, Rozycki M, Kirby J, Freymann J, Farahani K, Davatzikos C. Segmentation labels and radiomic features for the pre-operative scans of the tcga-gbm collection. the cancer imaging archive. *Nat Sci Data.* 2017;4:170117.
38. Bakas S, Akbari H, Sotiras A, Bilello M, Rozycki M, Kirby J, Freymann J, Farahani K, Davatzikos C. Segmentation Labels and Radiomic Features for the Pre-operative Scans of the TCGA-LGG collection [Data Set]. *The Cancer Imaging Arch.* 2017. <https://doi.org/10.7937/K9/TCIA.2017.GJQ7R0EF>.
39. Pieper S, Halle M, Kikinis R. 3d slicer. In: 2004 2nd IEEE International Symposium on Biomedical Imaging: Nano to Macro (IEEE Cat No. 04EX821). IEEE; 2004. p. 632–5.
40. Jenkinson M, Beckmann CF, Behrens TE, Woolrich MW, Smith SM. Fsl. *Neuroimage.* 2012;62(2):782–90.
41. Avants BB, Tustison NJ, Song G, Cook PA, Klein A, Gee JC. A reproducible evaluation of ants similarity metric performance in brain image registration. *Neuroimage.* 2011;54(3):2033–44.
42. Ali MB, Gu IY-H, Berger MS, Pallud J, Southwell D, Widhalm G, Roux A, Vecchio TG, Jakola AS. Domain mapping and deep learning from multiple mri clinical datasets for prediction of molecular subtypes in low grade gliomas. *Brain Sci.* 2020;10(7):463.
43. Chang K, Bai HX, Zhou H, Su C, Bi WL, Agbodza E, Kavouridis VK, Senders JT, Boaro A, Beers A, et al. Residual convolutional neural network for the determination of idh status in low-and high-grade gliomas from mr imaging. *Clin Cancer Res.* 2018;24(5):1073–81.
44. Yu J, Shi Z, Lian Y, Li Z, Liu T, Gao Y, Wang Y, Chen L, Mao Y. Noninvasive idh1 mutation estimation based on a quantitative radiomics approach for grade ii glioma. *Eur Radiol.* 2017;27(8):3509–22.
45. Zhang X, Tian Q, Wang L, Liu Y, Li B, Liang Z, Gao P, Zheng K, Zhao B, Lu H. Radiomics strategy for molecular subtype stratification of lower-grade glioma: detecting idh and tp53 mutations based on multimodal mri. *J Magn Reson Imaging.* 2018;48(4):916–26.
46. Chenjie Ge, Irene Yu-Hua Gu, Asgeir Store Jakola, Jie Yang. Deep Learning and Multi-Sensor Fusion for Glioma Classification Using Multistream 2D Convolutional Networks. *Annu Int Conf IEEE Eng Med Biol Soc.* 2018;2018:5894–7. <https://doi.org/10.1109/EMBC.2018.8513556>.

Publisher's Note

Springer Nature remains neutral with regard to jurisdictional claims in published maps and institutional affiliations.

Ready to submit your research? Choose BMC and benefit from:

- fast, convenient online submission
- thorough peer review by experienced researchers in your field
- rapid publication on acceptance
- support for research data, including large and complex data types
- gold Open Access which fosters wider collaboration and increased citations
- maximum visibility for your research: over 100M website views per year

At BMC, research is always in progress.

Learn more biomedcentral.com/submissions

